Pharmacogenomics and Personalized Medicine

Dovepress

open access to scientific and medical research

Open Access Full Text Article

ORIGINAL RESEARCH

Nidogen-2 (NID2) is a Key Factor in Collagen Causing Poor Response to Immunotherapy in Melanoma

Yan Sha[1,*], An-qi Mao[1,*], Yuan-jie Liu[2], Jie-pin Li[2], Ya-ting Gong[3], Dong Xiao[1], Jun Huang[1], Yan-wei Gao[1], Mu-yao Wu[3], Hui Shen[1]

[1]Departments of Dermatology, Zhangjiagang TCM Hospital Affiliated to Nanjing University of Chinese Medicine, Zhangjiagang, People's Republic of China; [2]Department of Oncology, Affiliated Hospital of Nanjing University of Chinese Medicine, Jiangsu Province Hospital of Chinese Medicine, Nanjing, People's Republic of China; [3]Departments of Rehabilitation, Zhangjiagang TCM Hospital Affiliated to Nanjing University of Chinese Medicine, Zhangjiagang, People's Republic of China

*These authors contributed equally to this work

Correspondence: Hui Shen; Mu-yao Wu, Email zjgzy046@njucm.edu.cn; wumuyao0613@163.com

Background: The incidence of cutaneous melanoma continues to rise rapidly and has an extremely poor prognosis. Immunotherapy strategies are the most effective approach for patients who have developed metastases, but not all cases have been successful due to the complex and variable mechanisms of melanoma response to immune checkpoint inhibition.

Methods: We synthesized collagen-coding gene expression data (second-generation and single-cell sequencing) from public Gene Expression Omnibus (GEO) and The Cancer Genome Atlas (TCGA) databases. Bioinformatics analysis was performed using R software and several database resources such as Metascape database, Gene Set Cancer Analysis (GSCA) database, and Cytoscape software, etc., to investigate the biological mechanisms that may be related with collagens. Immunofluorescence and immunohistochemical staining were used to validate the expression and localization of Nidogen-2 (NID2).

Results: Melanoma patients can be divided into two collagen clusters. Patients with high collagen levels (C1) had a shorter survival than those with low collagen levels (C2) and were less likely to benefit from immunotherapy. We demonstrated that NID2 is a potential key factor in the collagen phenotype, is involved in fibroblast activation in melanoma, and forms a barrier to limit the proximity of CD8+ T cells to tumor cells.

Conclusion: We clarified the adverse effects of collagen on melanoma patients and identified NID2 as a potential therapeutic target.

Keywords: Skin Cutaneous Melanoma, collagen molecules, *NID2*, bioinformatics, immunotherapy

Introduction

Skin Cutaneous Melanoma (SKCM) is a highly malignant tumor of melanocyte origin that occurs primarily in the skin and is the third most common type of skin malignancy.[1] According to the National Cancer Institute, by 2022, an estimated 99,780 new cases of melanoma will be diagnosed and 7650 patients will die from melanoma.[2] In recent years, with the rapid development of modern tumor immunology, immunotherapy for the development of SKCM has become a hot topic of current research.[3,4] The use of immune checkpoint inhibitors (ICIs) such as CTLA-4 inhibitors (ipilimumab)[5] or PD-1/PD-L1 inhibitors (nivolumab and pembrolizumab) has been highly successful in improving the prognosis of patients with SKCM.[6–8] It is worth noting that combining radiotherapy with immunotherapy can significantly enhance the immune stimulation potential to enhance the efficacy of immunotherapy.[9] Numerous studies have shown that anti-PD-1/PD-Ll therapy significantly improves objective response rates and survival in advanced malignant melanoma. Based on previously published data on the KEYNOTE-001 clinical trial study, the 5-year survival rate for all patients in the population included in this study was 34%, and for patients, on initial treatment with anti-PD-1 therapy, the 5-year survival rate was 41%, which provided a significant and clinically meaningful improvement in survival without distant metastases.[10,11] Nevertheless, immunotherapy does not benefit all patients, especially those with SKCM whose tumor tissue is not infiltrated by immune cells.

Received: 8 December 2022
Accepted: 25 February 2023
Published: 4 March 2023

Over the past decades, we have learned that the tumor microenvironment (TME) plays a significant role in tumor immunosuppression.[12,13] And the extracellular matrix (ECM), a core member of the TME, has become a hot research topic in recent years.[14–16] Increasingly, studies have shown that ECM is one of the major hurdles to obtaining successful cancer immunotherapy.[17,18] The ECM is a non-cellular three-dimensional macromolecular network consisting of collagen, proteoglycans (PGs)/glycosaminoglycans (GAGs), elastin, fibronectin (FN), laminin, and several other glycoproteins.[19] Whether in normal tissue or tumor, stromal components and cell adhesion receptors bind to each other to form a complex network that regulates a variety of cellular functions such as survival, growth, migration, differentiation, and immunity.[20] Numerous studies have shown that ECM promotes tumor cell growth, invasion, metastasis, and angiogenesis.[21] More importantly, the deposition of ECM leads to an increase in density and stiffness, thus resisting cell death and drug diffusion.[22] Collagen is one of the main components of the ECM and is involved in the structural formation of cancer fibrosis and solid carcinomas, together with stromal glycoproteins such as FN, laminin, elastin as well as versican.[23] This deposited collagen component is somewhat similar to the dense vegetation of a tropical rainforest or a 3D spider's web that wraps tightly around the outer edges of the tumor. This web-like structure formed by the collagen makes it more difficult for immune cells to squeeze through the web and enter the tumor.[24,25] Studies have shown that this heterogeneous collagen reduction can reprogram the tumor microenvironment, promote T-cell infiltration and improve prognosis.[26] Therefore, a deeper understanding of the relationship between collagen molecules and tumor immune responses will help to realize the potential of targeting ECM to improve cancer immunotherapy.

In this study, we analyzed the gene expression heterogeneity of 44 collagen molecules at the pan-cancer level, and the results showed that DNA methylation and copy number variation affect the expression of collagen molecules. We jointly analyzed information from multiple datasets sources to correlate collagen molecule activity with immunotherapy resistance. We developed a scoring system, called Col_Score, to quantify collagen molecules activity in SKCM. Integration of collagen molecules with prognosis and immunotherapeutic response is of great clinical importance.

Materials and Methods

Public Datasets

The RNA-seq transcriptome information and matching clinical data of 471 patients with Skin Cutaneous Melanoma (SKCM) patients have been acquired from the Cancer Genome Atlas (TCGA) portal website.[27] Validation data were downloaded from the Gene Expression Omnibus (GEO) database (GSE65904;[28] GSE15605;[29] GSE19234;[30] GSE59455;[31] GSE91061)[32] The Single-Cell RNA data included in this study were obtained based on an acral melanoma study (GSE189889).[33] All the gene expression data were obtained from the official portal and with the help of R software, the data matrix was established for subsequent assessments.

Consensus Clustering

We summarized data on collagen molecules from The Human Genome Organisation (HUGO) portal: *COL1A1, COL1A2, COL2A1, COL3A1, COL4A1, COL4A2, COL4A3, COL4A4, COL4A5, COL4A6, COL5A1, COL5A2, COL5A3, COL6A1, COL6A2, COL6A3, COL6A5, COL6A6, COL7A1, COL8A1, COL8A2, COL9A1, COL9A2, COL9A3, COL10A1, COL11A1, COL11A2, COL12A1, COL13A1, COL14A1, COL15A1, COL16A1, COL17A1, COL18A1, COL19A1, COL20A1, COL21A1, COL22A1, COL23A1, COL24A1, COL25A1, COL26A1, COL27A1*, and *COL28A1*. First, based on the expression level of 44 collagen molecules, unsupervised clustering analysis was used to identify the collagen phenotypes in melanoma, to classify patients. The optimal clustering number of melanoma-Cohort was determined by the consensus clustering algorithm, and its stability was verified. The R package "ConsensusClusterPlus" was used to perform each step, and the process was repeated 50 times (resampling rate 80%).[34]

Col_Score Evaluation

We used the principal components analysis (PCA) (orthogonal rotation) method in the "IOBR" package[35] to construct a scoring system to evaluate the levels of 44 collagen molecules in SKCM patients and named it Col_Score. The Col_Score formula is Col_Score = ∑(PC1+PC2).[36]

Enrichment Analysis

For the analyses of Gene Ontology (GO)[37] and Kyoto Encyclopedia of Genes and Genomes (KEGG) enrichment,[38] the METASCAPE tool was used.[39] Furthermore, with the "GSVA" package,[40] the differential signaling pathways principled on gene set variation analysis (GSEA) were also acquired. The HALLMARK gene set data resource was downloaded from the Molecular Signatures Database-MsigDB (www.broadinstitute.org/gsea/msigdb) as a background set.[41] $P < 0.05$ was considered important. In addition, the R package "Limma" was used to identify differentially enriched genesets between C1 and C2.

Immune Analysis

Based on the "IOBR" package, we calculated immune infiltration estimations for TCGA-SKCM samples with the Tumor Immune Estimation Resource (TIMER)(http://cistrome.shinyapps.io/timer), QUANTISEQ (http://icbi.at/quantiseq), XCELL (http://xCell.ucsf.edu/), and EPIC algorithms.[42] Heat maps demonstrating the differential abundance of immune cells were obtained by the "heatmap" R package. Tumor immune dysfunction and exclusion (TIDE) score[43] was determined for predicting the blockade response of potential immune checkpoint (ICB) in SKCM participants. Finally, the gene sets built into the 'IOBR' package were used to evaluate the various biological signal scores in melanoma samples and to compare the distribution in different collagen subtypes by Welch's *t*-test.

Cox Regression

The Univariate and multivariate Cox regression was applied to evaluate the hub genes' independent prognostic value.[44] Finally, the results were visualized by R with the forest plot including the hazard ratios (HRs), P-value, and 95% confidence intervals (CIs) of every variable.

Single-Cell Analysis

The Single-Cell RNA Sequencing (scRNA-seq) data GSE189889 was acquired from Gene Expression Omnibus (GEO) data.[45] All the data were incorporated into Seurat V3 and the obtained filtered cells were analyzed in Uniform Manifold Approximation and Projection (UMAP) and t-Distributed Stochastic Neighbor Embedding (t-SNE) after strict quality control of raw Unique molecular identifier (UMI) > 200, percentage of mitochondrial genes < 20%, log10 Gene per nUMI > 0.8). Then, by manual annotation, Hepatocyte from all cells was identified. The "FindAllMarkers" function (min.pct=0.25, logfc.threshold=1, tes.use="Wilcox") was adjusted for evaluating each cell type marker genes.[46] For plotting dplotslot and violin plots, "Dot plot" and "Vlnplot" functions were used. In addition, the "monocle3" package was used to infer potential evolutionary trajectories in fibroblasts.[47]

Construction of Co-Expression Networks

The R software package "multiscale embedded gene co-expression network analysis (MEGENA)" was applied to distinguish the co-expression network. MEGENA, is a method for assessing the co-expression module, was recently developed, and has novel advantages for the efficient construction of large-scale co-expression plane filtering networks and gene interaction preservation.[48] The construction of a fast planar filtered network (PFN) is the initial step in MEGENA analysis, followed by the computational determination of valuable PFN gene pairs, and finally, the aggregation of constructed PFNs for multiscale clustering analysis (MCA) for further evaluations. In addition, the degree values were measured for ranking the module genes to determine the potential hub genes.

Immunohistochemical Staining and Tissue Section Immunofluorescence Staining

Immunohistochemical (IHC) and Immunofluorescence staining followed the method described in the previous study.[49,50] The antibodies used are listed in Supplementary Table 1. The concentrations used were based on those used in previous research or on the manufacturers' recommendations. After blocking tissue sections with protein blocking solution, slides were incubated with primary antibody. IHC results (intensity and extent of staining) were independently scored by two observers. The images were captured using a NIKON Eclipse Ni-E microscope (NIKON, Japan). Staining intensity was graded as follows: 0, negative staining; 1, weak staining; 2, moderate staining; and 3, strong staining. The extent of staining was scored based on the proportion

of positively stained cells per specimen, as follows: 0, no positively stained cells; 1 <10% positively stained cells; 2, 10–50% positively stained cells; and 3, >50% positively stained cells. The histochemistry score (H-SCORE), which represents the proportion of positively stained cells and the intensity of expression, was calculated as follows: H-SCORE= ∑(PI × I) = (percentage of cells with weak intensity × 1) + (percentage of cells with moderate intensity × 2) + (percentage of cells with strong intensity × 3). In the formula, PI represents the percentage of positive cells to the total number of cells in a particular field and I represent the intensity of staining. The H-SCORE ranges from 0 to 300, with a higher score representing stronger positive staining.[51]

After blocking in 5% bovine serum albumin in phosphate-buffered saline, 0.1% Tween was followed by an overnight incubation (4 °C) with the primary antibody. This procedure was followed by incubation with the secondary antibodies. Nuclei were stained using 4',6-diamidino-2-phenylindole (DAPI) for 3 min, and the cells were incubated in the dark for 3 min. The slides were washed with phosphate-buffered saline (PBS) four times, for 5 min each. Then, the slides were sealed with a sealing solution containing a fluorescence quencher and observed and imaged with an inverted fluorescence microscope (Olympus CKX-41, Japan).

Inclusion/Exclusion Criteria for Participants and Sample Collection

The use of specimens was carried out with the informed consent of the patients in accordance with the principles of the Declaration of Helsinki.[52] All patient records/information was anonymized and de-identified prior to analysis. Each sample was collected frozen and immediately stored in liquid nitrogen. Inclusion criteria: (1) All patients were diagnosed as SKCM for the first time by pathology. (2) The diagnosis was referenced in the latest (8th edition) American Joint Committee on Cancer (AJCC) SKCM staging system.[53] (3) Patients with SKCM who were hospitalized in the Department of Dermatology and Oncology of Zhangjiagang TCM Hospital Affiliated to Nanjing University of Chinese Medicine from 2020-01-01 to 2022-01-01. Also, pathological specimens from each melanoma patient were kept for independent re-diagnostic confirmation by two doctors. (4) All patients had complete clinical information. Exclusion criteria: (1) Patients with a clinical diagnosis of a tumor that has metastasized to the skin from another site. (2) Exclusion of any other serious chronic disease or other visceral tumors. (3) Incomplete clinical data. Finally, a total of 40 patients with SKCM were analyzed.

Identification of Differentially Expressed Genes in SKCM

By applying the "Limma" package,[54] the differentially expressed genes (DEGs) were determined. DEGs, which had a P value <0.05 and absolute log2 fold change (FC) >2, were contemplated as statistically important, which were then subsequently used for future analyses.

Expression and Survival Analysis

In the public dataset, the mortality was assessed through survival analysis visualized by the "survival" R package, which mainly includes progression-free interval (PFI), overall survival (OS), and disease-specific survival (DSS). Furthermore, paired samples in TCGA-SKCM differences were assessed by paired *t*-test, and via the "ggplot2" package all the results were visualized.[55]

Reagents

The Supplementary Material enlists all the antibodies and reagents used in this investigation (Supplementary Table 1). Antibodies dilutions were prepared by following either previous research or by the recommendations provided by the manufacturer.

Statistical Analysis

We used Spearman correlation coefficients to determine the correlation between variables. The Welch's *t*-test was used to estimate the statistical significance of normally distributed variables, and the Mann–Whitney *U*-test (also known as the Wilcoxon rank sum test) was used to analyze non-normally distributed variables. To compare two or more groups, Kruskal–Wallis and one-way ANOVA tests were used. The log-rank (Mantel-Cox) test was used to determine statistically significant differences. A univariate Cox proportional hazard regression model was used to calculate the hazard ratio. All statistical analyses used R (https://www.r-project.org/), with a P value < 0.05 (two-tailed) indicating significant differences.

Results

Transcriptional Variation and Functional Characterization of 44 Collagen Molecules

We obtained basic information on 44 collagen molecules from Human Genome Organization (HUGO). Figure 1A demonstrates the function of collagen in providing a physical barrier to tumor cells from attack by the immune system. We selected 4394 samples with at least one collagen molecule mutation from the TCGA database to observe the transcriptomic variation of collagen molecules at the pan-cancer level. The 10 collagen molecules with the highest somatic mutation frequencies were *COL11A1, COL6A3, COL22A1, COL12A1, COL6A6, COL7A1, COL5A1, COL4A4, COL14A1*, and *COL3A1* (Figure 1B). Out of 4395 samples, 2726 samples had collagen mutations with a frequency of 62.04%. The highest mutation frequency was found in *COL11A1* (16%), followed by *COL6A3* (14%) and *COL22A1* (13%), missense mutation was the most common type of genomic alteration, and melanoma (TCAG-SKCM) was the most common type of cancer. Our results suggested that transcriptome variation is one of the important factors affecting collagen molecule levels. In most cancer types, copy number variation (CNV) and mRNA expression levels were positively correlated, especially in *COL8A2* (Figure 1C), while DNA methylation levels were negatively correlated with mRNA expression levels, especially in *COL1A1* (Figure 1D). Analysis of SNV frequency showed that the single nucleotide variant (SNV) frequencies of 44 collagen molecules in the pan-cancerous tissues varied significantly, with the highest frequency of *COL11A1*, especially in SKCM (Figure 1E). We noted that in pan-cancer, almost all collagen molecules exhibited a consistent activating effect on EMT (Figure 1F). This part of the results suggests that collagen molecules are highly transcriptionally heterogeneous in various cancers and their abnormal expression is closely associated with genomic alterations.

We next focus on the significance of collagen molecules in melanoma. Interestingly, we found frequent mutational co-occurrence between collagen molecules, such as *COL24A1* and *COL9A3* mutations, while exclusive mutation events were hardly observed (Figure 2A). Among the 104 samples, 79 samples carried mutations in collagen molecules, with a mutation frequency of 75.96%, and *COL22A1* had the highest mutation frequency, which was mainly missense mutation (Figure 2B). In melanoma tissues, most collagen molecules inhibited the DNA damage response, but there was no consistent effect on the cell cycle, EMT, hormone AR signaling pathway, and RAS/MAPK signaling pathway (Figure 2C). The TCGA-SKCM data suggested an extensive co-expression relationship between collagen molecules (Figure 2D). To ensure the stability of the results, we integrated data from the Gene Expression Omnibus (GEO) database, including 565 melanoma samples, and corrected for batch effects using the "Combat" algorithm in the SVA package. The gene expression baseline for each cohort was shown before (Figure S1A) and after (Figure S1B) the batch effect. Subsequently, we observed similar results to TCGA in the mGEO data (Figure S2). Finally, we confirmed the localization of collagen expression by using a single-cell RNA-seq dataset containing 35,988 single cells of melanoma samples. We annotated the cells by marker genes specific to each cell type (Figure S3A–C), and the results showed that collagen molecules are highly expressed on fibroblasts (Figure 2E–G).

Two Different Collagen Clusters Identified by Unsupervised Learning

To further understand the heterogeneity of collagen in melanoma, unsupervised consensus analysis was used to classify the 471 samples in TCGA-SKCM into two different subtypes with different molecular and clinical characteristics, including 194 samples in cluster 1 and 277 samples in cluster 2, based on the mRNA expression levels of 44 collagen molecules (Figure 3A and B). Figure S4A showed that we can obtain the satisfactory clustering effect when $k = 2$. The PCA showed that the two clusters can be well distinguished from each other (Figure 3C). The heatmap showed that the levels of collagen molecules differed between the two clusters and that the levels of collagen molecules were significantly higher in C1 than in C2 (Figure 3D). Notably, C1 contained more patients with advanced stage than C2 (Figure 3E). Survival analysis also showed that patients in C1 had a more unfavorable prognosis, including overall survival (OS) and disease-specific survival (DSS), than those in C2 (Figure 3F and G, $P < 0.05$, logrank test). To ensure the stability of the clustering, the same process was performed based on the mGEO data (Figures S5A–H and S4B). These results suggested that collagen expression patterns were heterogeneous in melanoma and were strongly associated with the clinical outcomes of melanoma patients.

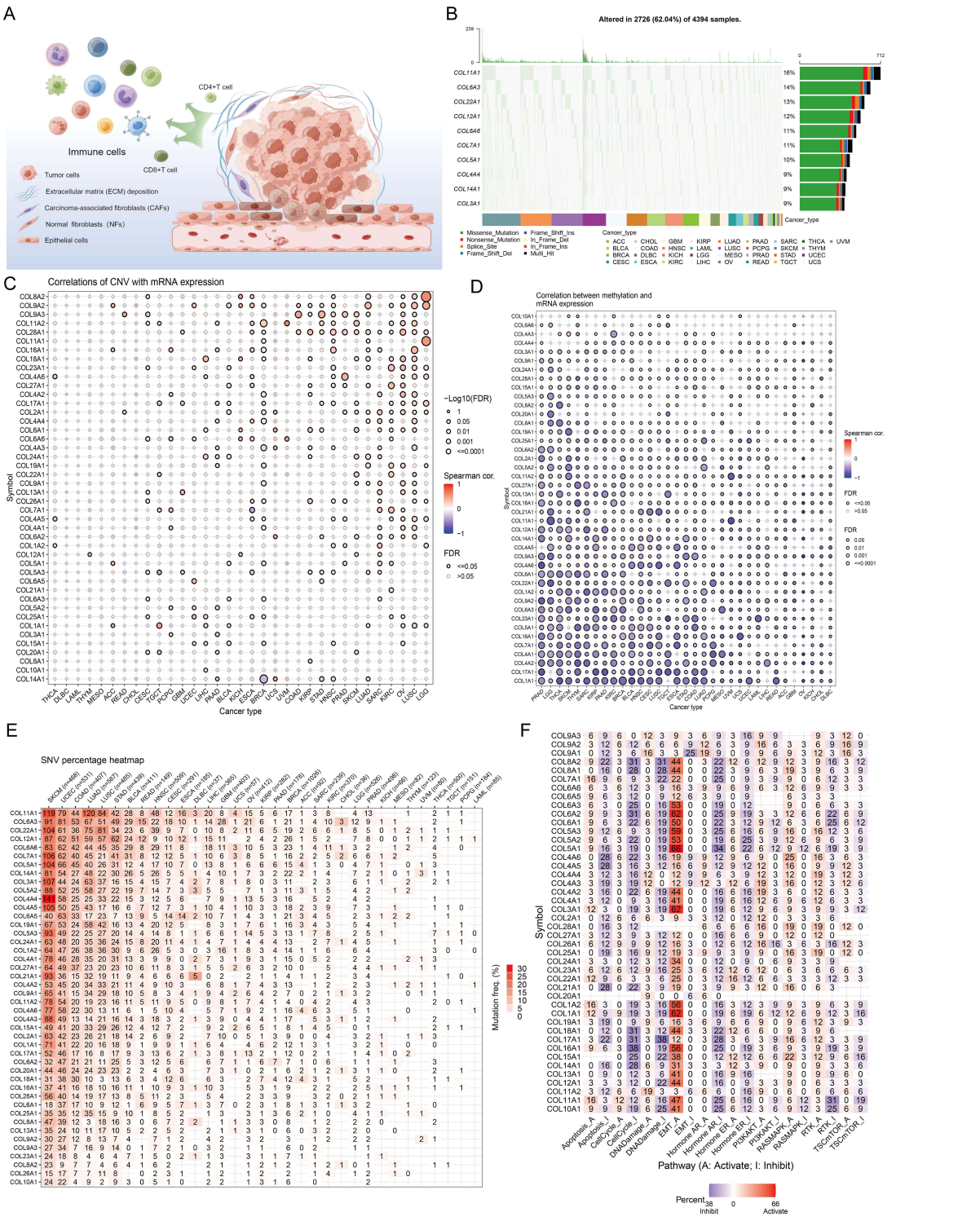

Figure 1 Expression variation of collagen molecules in pan-cancer. (**A**) The pattern map was drawn to show the molecular regulation mechanism of the extracellular matrix (ECM) and its potentially important regulatory role in the tumor immune microenvironment. (**B**) The waterfall diagram shows the somatic mutations of the 10 collagen molecules with the highest mutation frequency using pan-cancer analysis. 62.04% is the proportion of 2726 samples with at least one mutation of the top 10 genes among 4394 samples with at least one mutation of 44 collagen molecules. The percentage figure of each line on the right of the picture is the number of samples with the corresponding gene mutation divided by 4394 samples with at least one mutation among the 44 collagen molecules. (**C**) The bubble chart shows the correlation between copy number variant (CNV) and mRNA expression level. Red indicates a positive correlation; blue indicates a negative correlation. The deeper color indicates a larger correlation index. The bubble size indicates the false discovery rate (FDR). (**D**) The bubble chart shows the correlation between DNA methylation of the 44 collagen molecules and mRNA expression. Red shows a positive correlation and blue shows a negative correlation. The darker color indicates a larger correlation index. Bubble size indicates the FDR. (**E**) The heatmap inferring the genetic relationship using single-nucleotide variations (SNV) data from The Cancer Genome Atlas (TCGA) pan-cancer database. The darker the color, the higher the percentage in the sample. (**F**) Mutation frequency of 44 collagen molecules in 471 patients with Skin Cutaneous Melanoma (SKCM) in the TCGA-SKCM cohort. Each column represents an individual patient.

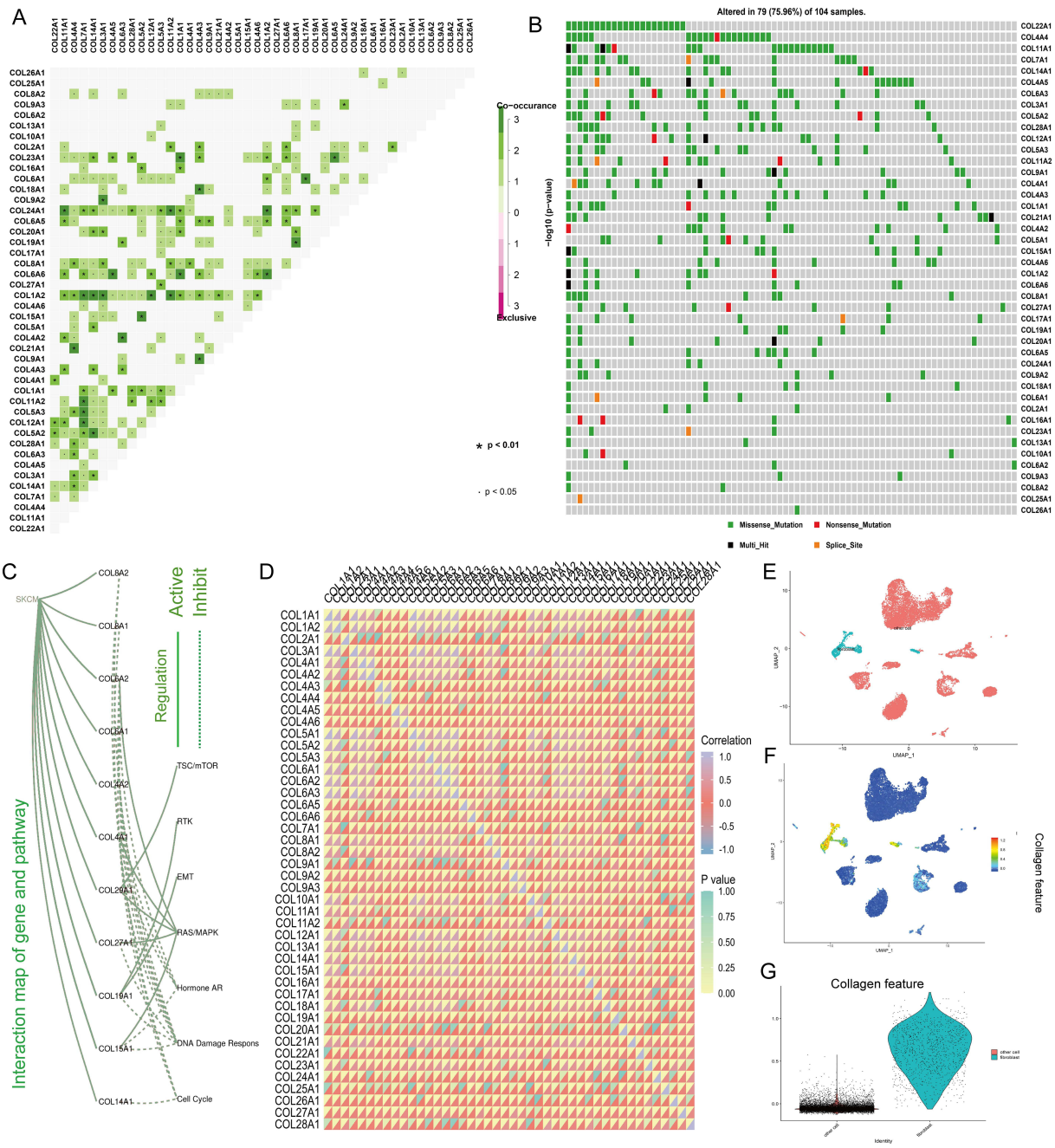

Figure 2 Expression variation of collagen molecules in SKCM. (**A**) Mutation characteristics of the 44 collagen molecules in 104 patients with SKCM in the TCGA-SKCM cohort; green indicates co-mutation, brown indicates mutex-mutation, the asterisk indicates P-value (*P <0.01, •P <0.05). (**B**) The heatmap shows the correlation between the expression level of the 44 collagen molecules in important cancer signaling pathways. The global percentage of cancers in which a gene has an effect on the pathway among the 32 cancer types, is shown as the percentage: (number of activated or inhibited cancer types/32 *100%). Heatmap shows collagen molecules that have a function (inhibit or activate) in at least 5 cancer types. "Pathway activate" (red) represents the percentage of cancers in which a pathway may be activated by given genes, inhibition in a similar way shown as "pathway inhibit" (blue). (**C**) The correlation between the 40 collagen molecules in SKCM and important cancer signaling pathways. The solid line represents activation and the dashed line represents inhibition. (**D**) Correlation between expression levels of 40 collagen molecules, red represents positive correlation, blue represents negative correlation, and shades of yellow indicate the P values. (Spearman method, TCGA-SKCM, n = 471). (**E**) Cells were clustered into 2 types via Uniform Manifold Approximation and Projection (UMAP) plot dimensionality reduction algorithm. Fibroblast was distinguished from all other cells based on UMAP dimensionality reduction analysis. (**F**) UMAP visualization of the collagen feature. (**G**) Violin plots of the collagen feature.

Biological Signaling Differences in Collagen Phenotypes

We analyze here the differences in gene expression between collagen subtypes and explore the characteristics of the associated biological signatures. GSVA enrichment analysis revealed differences in enrichment pathways between C1 and C2, and specifically, EMT and angiogenesis were significantly highly enriched in C1 (Figure 4A). We obtained DEGs

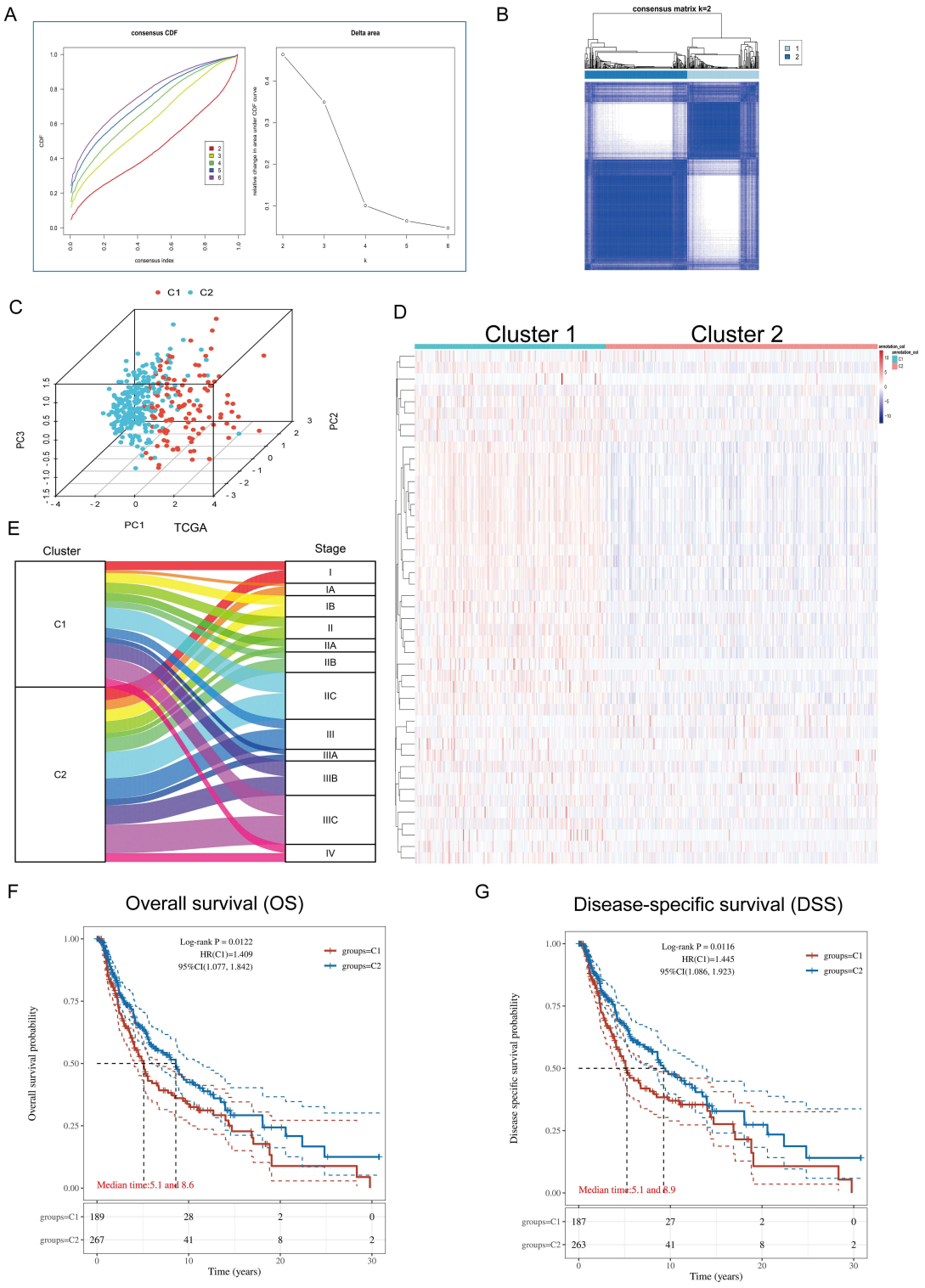

Figure 3 Unsupervised Machine Learning algorithms was used to identify 2 molecular subtypes in TCGA-SKCM. (**A**) Left: The cumulative distribution function (CDF) curves in consensus cluster analysis. CDF curves of consensus scores by different subtype numbers (k = 2, 3, 4, 5, and 6) were displayed. Right: Relative change in area under the CDF curve for k = 2–6. (**B**) The consensus score matrix of all samples when k = 2. The higher the consensus score was, the more likely they were assigned to the same group based on TCGA-SKCM. (**C**) The Principal Component Analysis (PCA) distribution of TCGA-SKCM samples by the expression profile of collagen molecules. Each point represents a single sample; different colors represent the C1 and C2 subtypes respectively. (**D**) Expression distribution of 44 collagen molecules between two subtypes based on TCGA-SKCM. (**E**) The Sankey diagram fully demonstrated the association between Clinicopathological and subtypes attributes. (**F** and **G**) Survival analysis including Overall Survival (OS) and Disease-Specific Survival (DSS) based on 2 subtypes (TCGA-SKCM, Logrank test, n = 471).

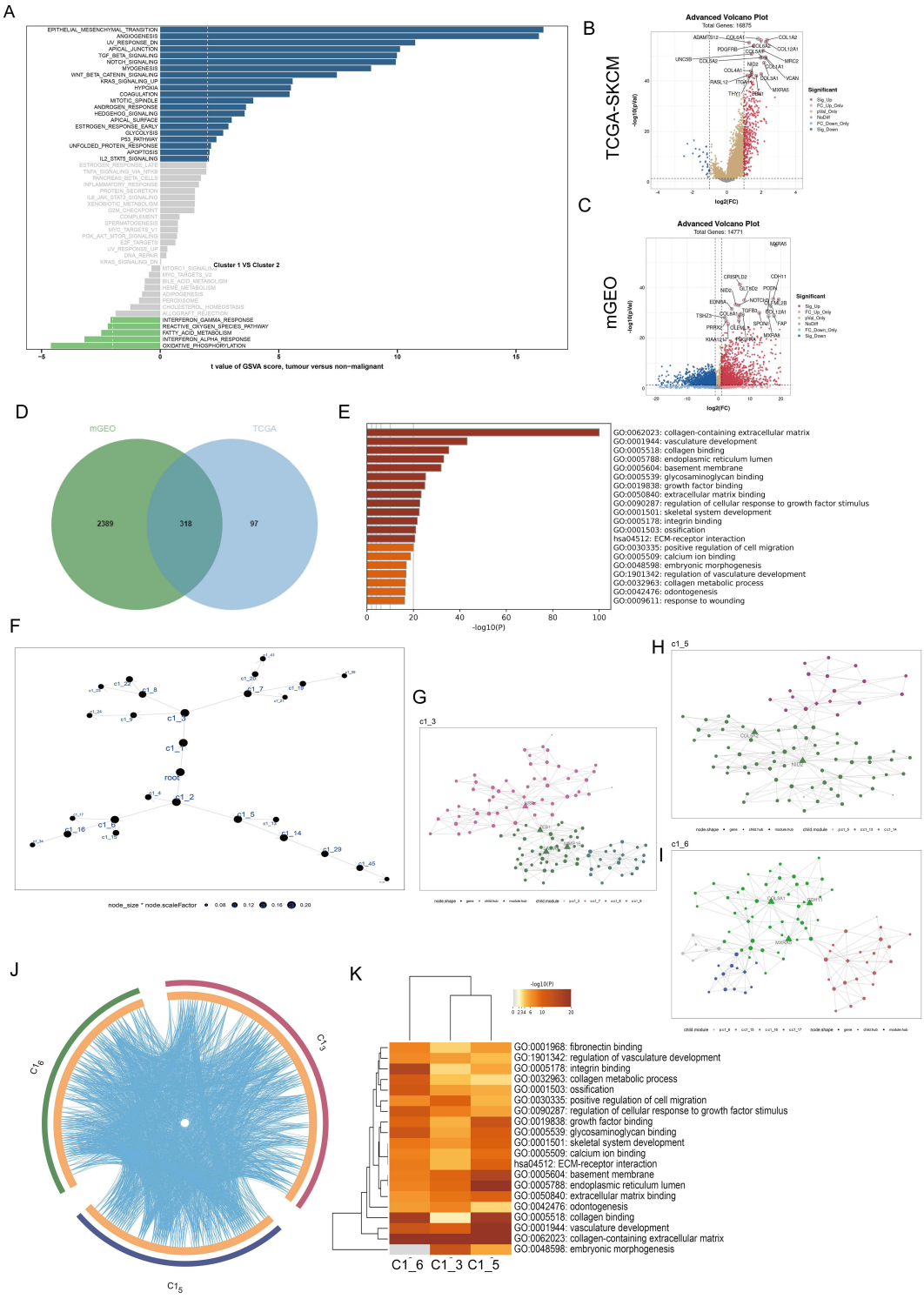

Figure 4 Analysis of collagen-related signaling pathways. (**A**) Gene Set Variation Analysis (GSVA) enrichment analysis shows the activation status of biological pathways between 2 different collagen subtypes. Bar plots were used to visualize the HALLMARK geneset, with blue representing activation and green representing inhibition in C1. Gray regions stand for not statistically significant. (**B** and **C**) Volcano map of differentially expressed genes (DEGs) between C1 and C2 based on TCGA-SKCM (**B**) and mGEO (**C**) dataset. Data on the abscissa are differences in gene expression (log2 fold change); data on the ordinate represent the significance of these differences (−log10 padj). Red indicates upregulation in C1, and blue indicates downregulation in C1. (**D**) Venn diagram indicates the intersecting genes of two independent datasets. (**E**) Significant Gene Ontology (GO) enrichment terms and Kyoto Encyclopedia of Genes and Genomes (KEGG) pathway enrichment analyses of the overlap genes. Each row represents one cluster and color indicates significance. Heatmap shows the top 20 clusters correlated with the intersecting genes. (**F**) The co-expression network of intersecting genes is based on Multiscale Embedded Gene Co-Expression Network Analysis (MEGENA). Each node represents a module, with the larger nodes indicating a higher number of genes. (**G**–**I**) The MEGENA network shows the top three gene modules. The larger the size, the more important it is in the network ((**G**)C1_3; (**H**) C1_5; (**I**) C1_6). (**J**) Circos plot representing the intersections of the top three gene modules. The outermost circle is colored to represent different samples, the inner circle is Orange for each sample-specific gene, and the blue line indicates gene intersections. (**K**) GO and KEGG enrichment analysis of the top three gene modules. Each row represents one cluster; color indicates significance, and gray color indicates non-significance. Heatmap showing the top 20 clusters correlated with the top three gene modules.

https://doi.org/10.2147/PGPM.S399886 DovePress

between the two clusters based on TCGA-SKCM (Figure 4B) and mGEO (Figure 4C), respectively, and enrichment analysis indicated that the intersecting genes were involved in ECM-related signaling pathways (Figure 4D and E). To identify possible regulatory mechanisms in the collagen phenotype, we constructed a MEGENA network using the above intersecting genes (Figure 4F). As shown in Figure 4G–I, among all gene modules, the largest module C1_3 consists of 122 genes, followed by C1_6 and C1_5 with 91 and 83 genes, respectively. These three gene modules were closely linked to each other (Figure 4J) and were all highly correlated with ECM-related signals (Figure 4K). Finally, we included the obtained hub genes in the COX regression to identify reliable prognostic factors and we found that both *NID2* and *ZEB1* were unfavorable factors for survival in melanoma patients (Figure 5A–C), interestingly, the levels of *NID2* were higher in patients who had developed metastases (Figure 5D). The results suggested that *ZEB1* and *NID2* may be potentially important regulators of the collagen phenotype.

Single-Cell Analysis of *NID2*

As a hot molecule in cancer research, there is considerable evidence that *ZEB1* is involved in various biological processes to promote the growth and metastasis of various tumors, including melanoma. Thus, we focused our attention on *NID2*, which has not yet been characterized in melanoma. All cells were processed with Uniform Manifold Approximation and Projection (UMAP) and divided into 20 clusters Figure 6A and the expression of *NID2* at the single cell level was shown in Figure 6B. To further determine the possible functions of *NID2*, fibroblasts were distinguished from other cells and divided into 6 clusters (Figure 6C). Both TCGA and GEO data showed a high positive correlation between *NID2* levels and fibroblast abundance (Figure 6D; TCGA, $r = 0.736$, $P < 0.001$; mGEO, $r = 0.610$, $P < 0.001$; MCPcounter). Pseudotime analysis suggested an evolutionary route from Cluster 0 to Cluster 2 in fibroblasts, and enrichment analysis indicated that Cluster 2 functions involved the cytoskeleton, focal adhesion, and blood vessel development (Figure 6E and F). We next compared the trends in the levels of *NID2* and several fibroblast activation markers and found that the trends of *NID2* and *ACTA2, CAV1* were highly consistent, suggesting that *NID2* may be involved in the activation process of fibroblasts (Figure 6G and H). These results provided solid evidence that NID2 expression level was closely associated with specific stromal cell types (fibroblasts).

Variation in the Infiltration Characteristics of TME Cells in Collagen Phenotype

We further analyzed the effect of collagen on the tumor immune microenvironment of s. Our results show that only fibroblasts and endothelial cells were highly enriched in C1, while immune cell abundance hardly differed between the two clusters (Green Box; Figure 7A, TCGA; Figure 7B, mGEO). To clarify whether collagen affects the abundance of immune components, we compared the differences in the expression of immune cytokines including chemokines, interleukins, interferons, etc. between the two clusters. The results were consistent with what we had envisioned-no significant differences were observed (Figure 7C, TCGA; Figure 7D, mGEO). These results imply that the expression of collagen molecules in melanoma may only affect the abundance of tumor stroma. We evaluated the TME score using the "ESTIMATE" package and showed that stromal scores were significantly higher in C1 than in C2, while results on immune scores and immune checkpoint levels were inconsistent in the two independent datasets (Figure 7E, TCGA; Figure 7F, mGEO). Pathological sections confirmed that C1 exhibited a significantly high abundance of stromal components (Figure 7G). Considering that the tumor stroma is a key barrier to the success of immunotherapy, we finally explored the impact of collagen phenotype on immunotherapy by the tumors immune dysfunction and exclusion (TIDE) algorithm (Figure 7H) and the cohort of immunotherapy (Figure 7I), respectively, and found that patients in C1 may have more difficulty benefiting from immunotherapy compared to those in C2. The results further confirmed that C1 was critically characterized by a high abundance of collagen matrix compared to C2, and affected the expected effect of immunotherapy.

Clinical Significance of Col_Score

The above results confirm the importance of collagen phenotype for tumor stroma and survival of melanoma patients. We constructed a collagen molecule-based scoring model to quantify collagen abundance, called Col_Score. The Col_Score in C1 is significantly higher than that in C2 based on TCGA (Figure 8A, Welch's *t*-test, P = 4.09e-79) and mGEO (Figure 8B, Welch's *t*-test, P = 4.18e-92). We assigned patients in the TCGA-SKCM and mGEO cohorts to high or low

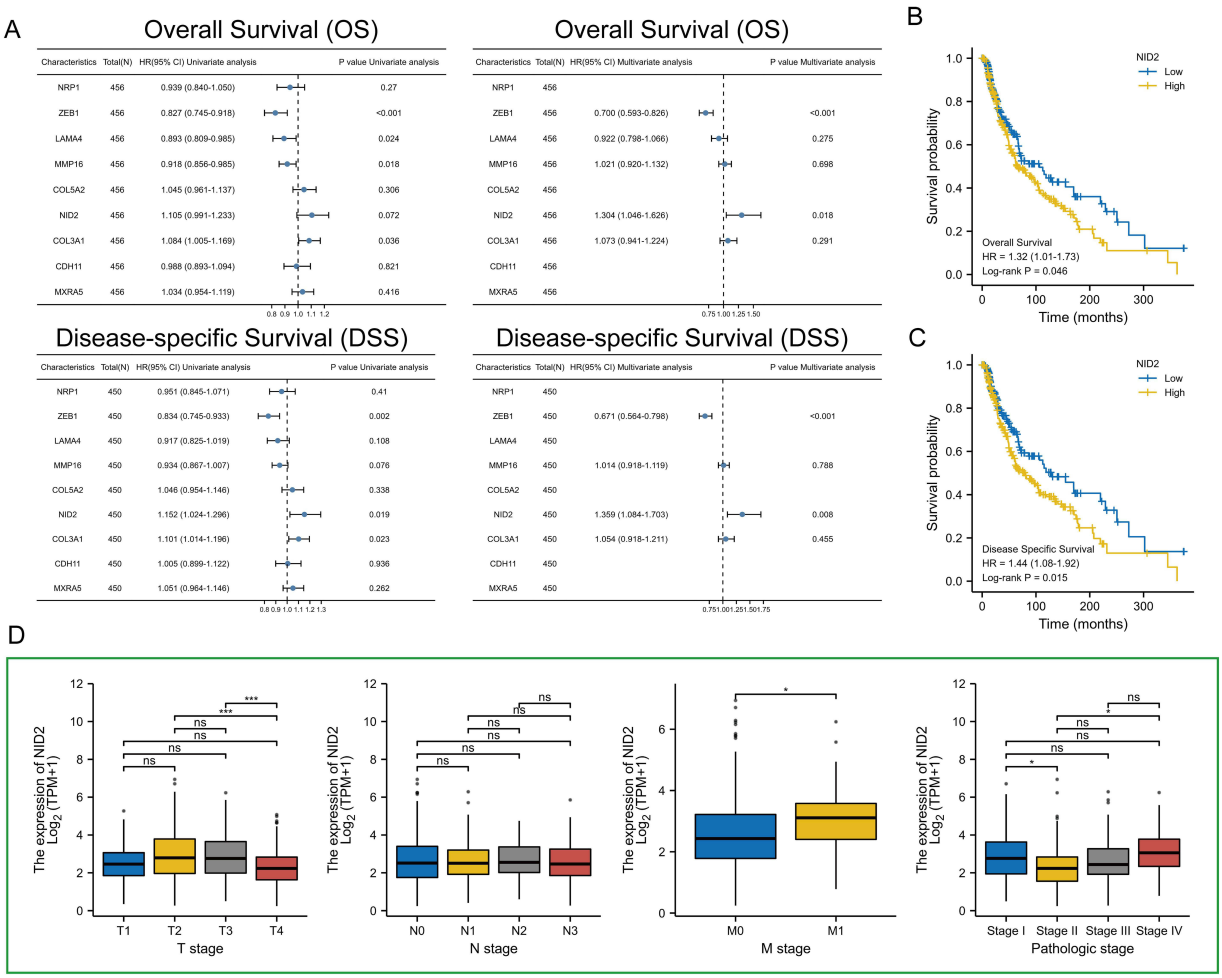

Figure 5 Identification of NID2 as a key factor in the collagen phenotype. (**A**) Univariate and multivariate COX model showing an association between hub DEGs expression and OS as well as DSS in SKCM. (**B** and **C**) The Kaplan-Meier survival analysis including OS, and DSS based on *NID2* expression levels in TCGA-SKCM (n = 471). Logrank test was performed. (**D**) Association of *NID2* expression with T (Tumor), N (Node), and M (Metastasis) stages and pathologic stage of SKCM patients (n = 471). *P < 0.05, ***P < 0.001.
Abbreviation: NS, not significant.

Col_Score group based on median Col_Score levels and found that Col_Score was a detrimental factor for survival in melanoma patients, including OS (TCGA, P = 0.03; mGEO, P = 0.014), PFS (mGEO, P = 0.019), and DSS (TCGA, P = 0.024; mGEO, P = 0.028) (Figure 8C–G). Col_Score was positively correlated with the level of infiltration of fibroblasts, endothelial cells, monocytes/macrophages, and neutrophils, but not with the number of almost all types of T cells (Figure 8H). In addition, Col_Score was positively correlated with EMT, CAFs, and ICB resistance signal scores, but not with immune checkpoint scores (Figure 8I). Finally, pathological sections confirmed that the high Col_Score group showed a higher stromal component (Figure 8J and K), again indicating a strong positive correlation between collagen and tumor stroma.

Characterization of NID2 as a Marker of Fibroblast Activation and Correlation with Immune Exclusion Phenotype

Since the above results suggested that NID2 may play a crucial role in fibroblast activation. Immunofluorescence (IF) staining results directly confirmed that the expression of NID2 was highly consistent with ACTA2 (Figure 9A). Subsequently, we found in IF staining of SKCM samples that NID2 could form a barrier to prevent CD8+ T cells from entering the tumor tissue to exert their killing effect (Figure 9B). Concurrently, we calculated the correlation between the *NID2* and the TIDE score and found TIDE score was positively correlated with the *NID2* expression level (Figure 9C TCGA-SKCM, r = 0.34, P < 0.001, Spearman). Since the predicted results

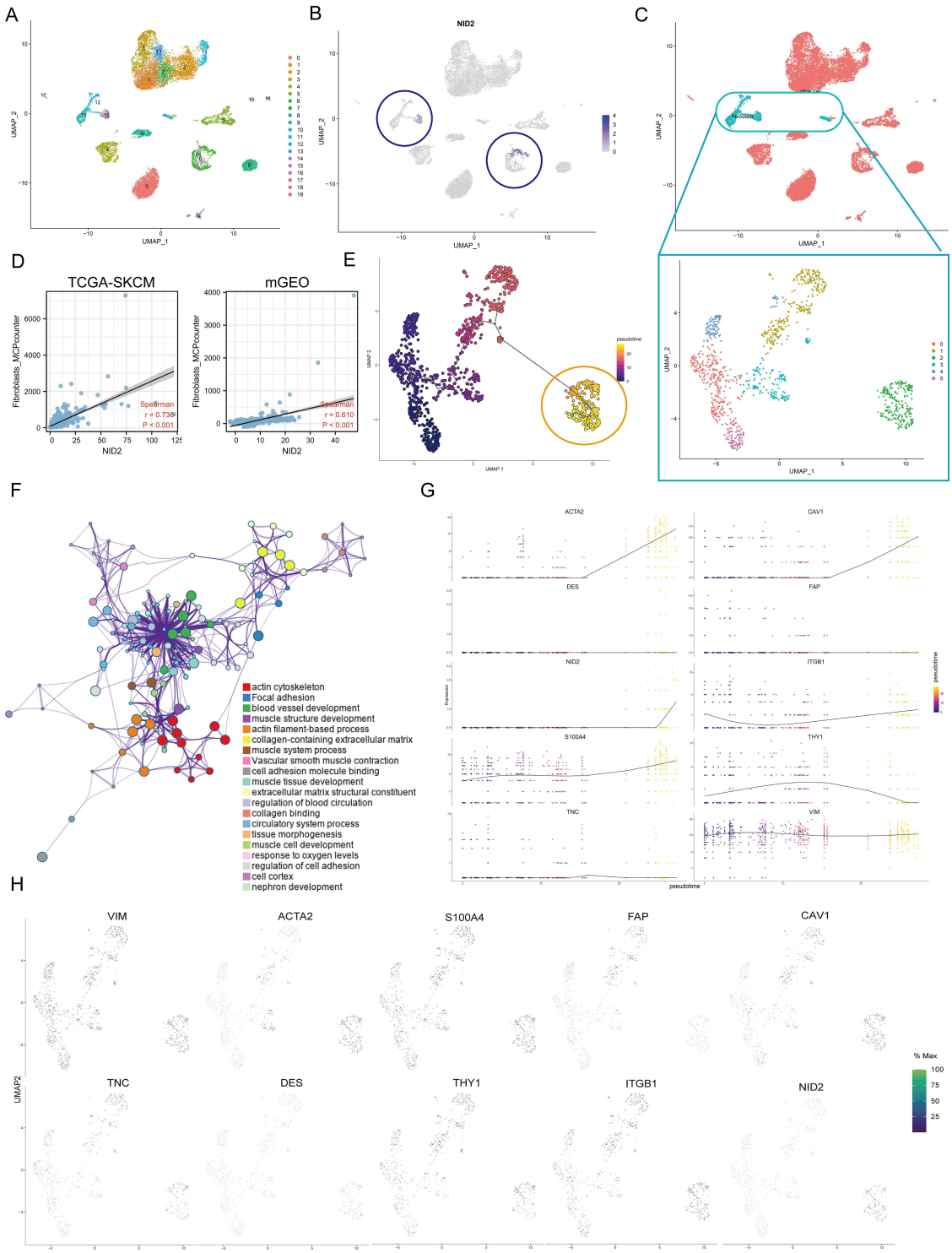

Figure 6 Single-cell analysis. (**A**) Cells were clustered into 20 types via UMAP. (**B**) Dot plots demonstrate the expression distribution of *NID2*. (**C**) UMAP plot dimensionality reduction algorithm, each color represents a unique cluster. Fibroblasts are distinguished from all other cells based on UMAP dimensionality reduction analysis. (**D**) Correlation analysis of the Fibroblasts and *NID2* mRNA expression levels based on TCGA-SKCM, and mGEO datasets. (**E**) Pseudotime trajectory of all the fibroblasts. The Orange circle indicating Cluster 5 identified by Seurat and all the fibroblasts were colored by their assigned pseudotime values. (**F**) Functional enrichment analysis of Cluster 5. (**G**) Jitter plots show the expression level of the fibroblast activation markers and *NID2* changing with pseudotime. (**H**) UMAP dimensionality reduction visualizes the similarity of expression profiles of *NID2* and 9 fibroblast activation markers.

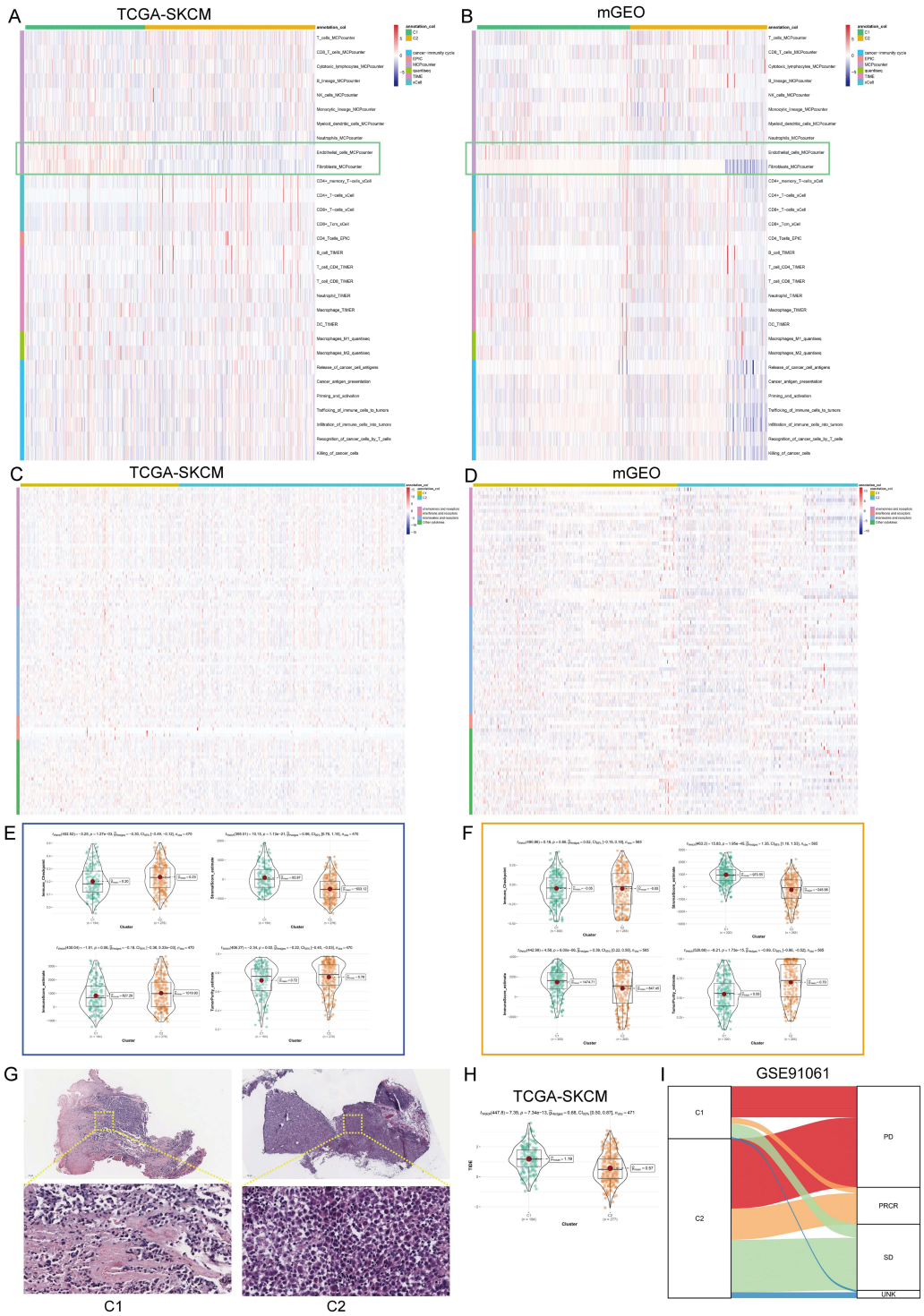

Figure 7 Variations in immune-related genes and the infiltration characteristics of TME cells in 2 collagen molecules phenotypes. (**A** and **B**) The thermogram shows the frequency of TME infiltrating cells and immune score in 2 collagen molecules phenotypes ((**A**) TCGA-SKCM; (**B**) mGEO). (**C** and **D**) The thermogram shows variations in mRNA expression of chemokines, interferons, interleukins, and other cytokines between the 2 levels of collagen molecules ((**C**) TCGA-SKCM; (**D**) mGEO). (**E** and **F**) The violin plots specifically showed the differences between C1 and C2 in terms of the immune checkpoint, immune score, stromal score, and tumor purity (Welch's *t*-test; (**E**) TCGA-SKCM, (**F**) mGEO). (**G**) Representative pictures of pathological Hematoxylin-eosin (HE) staining of C1 and C2 (Scale bars, 500 and 20 μm (enlarged images). (**H**) The differences in tumor immune dysfunction and exclusion (TIDE) score between C1 and C2 based on TCGA-SKCM. (**I**) The Sankey diagram fully demonstrated the difference in response to immunotherapy between different two 2 subtypes based on GSE91061.

Abbreviations: CR, complete response; PR, partial response; SD, stable disease; PD, progressive disease; UNK, unknown.

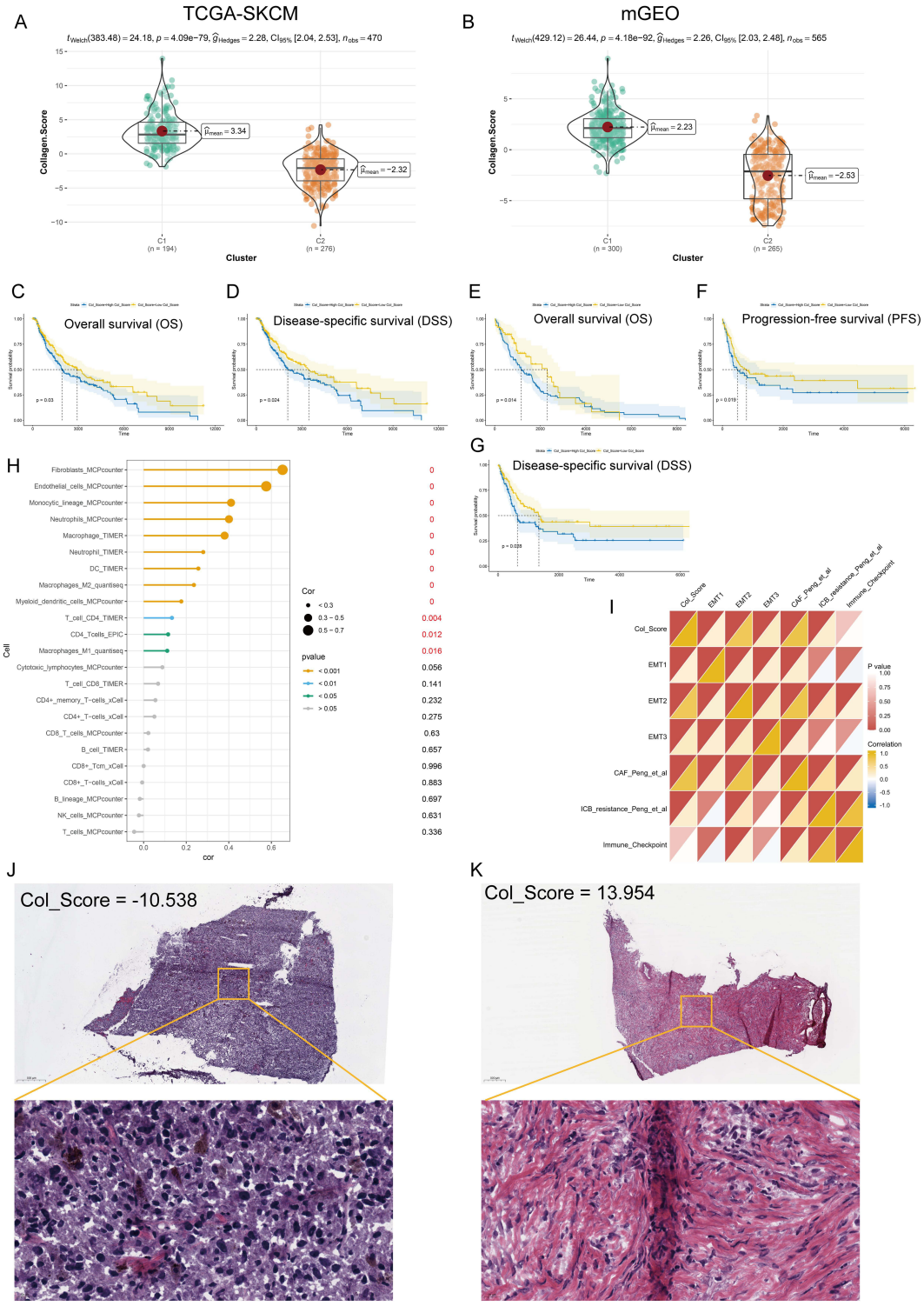

Figure 8 Clinical significance of Col_Score. (**A** and **B**) The violin plots show the Col_Score difference between 2 different collagen subtypes. The line in the box represents the mean value ((**A**) TCGA-SKCM; (**B**) mGEO). (**C**–**G**) The Kaplan-Meier curve shows a significant difference in the survival rate between high and low Col_Score groups ((**C** and **D**) TCGA-SKCM, logrank test, n = 471; (**E**–**G**) mGEO, logrank test, n = 545). (**H**) The bubble chart shows the correlation between the Col_Score and the level of immune cell infiltration. The color indicates the P-value. The bubble size indicates the degree of correlation; with larger bubbles indicating a stronger correlation. (**I**) The chart shows the correlation between the Col_Score and Epithelial-mesenchymal transition (EMT), Cancer-Associated-Fibroblasts (CAFs), Immune checkpoint blockade (ICB) resistance, and immune checkpoint. Yellow represents a positive correlation, blue represents a negative correlation. The smaller the P-value, the deeper the red color. (**J** and **K**) Image representing the pathological HE staining variation between the low (**J**) and high (**K**) Col_Score groups (Scale bars, 500 and 20 μm enlarged images).

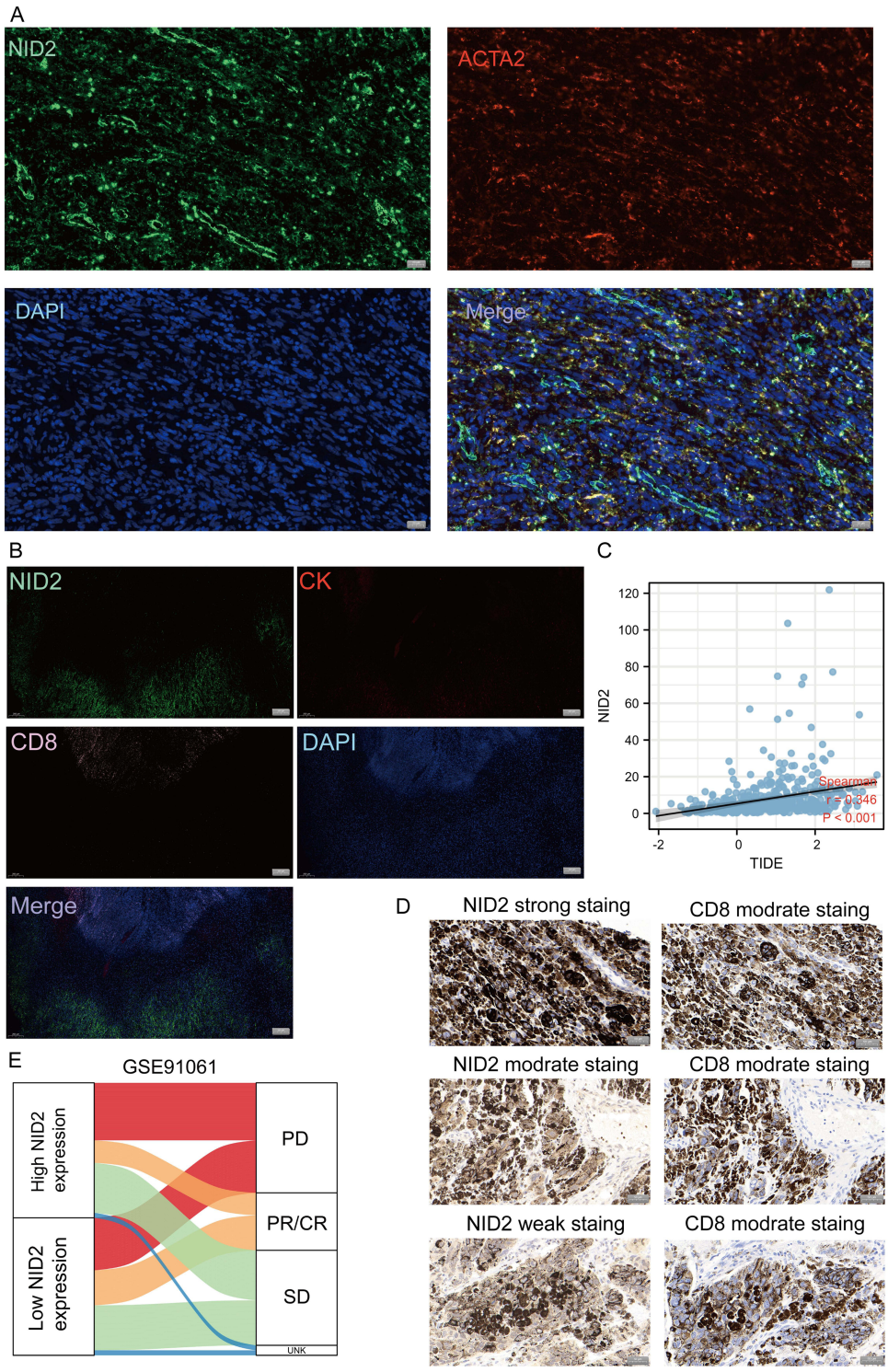

Figure 9 NID2 is related to the tumor immune microenvironment. (**A**) Double immunofluorescence staining images of NID2 and ACTA2 in the SKCM tissue. The representative view of the co-staining of NID2 and ACTA2 is shown in the enlarged image view below. Nuclei (DAPI) in blue (Magnification, ×400, scale bars = 20 μm). (**B**) Correlation between *NID2* mRNA expression level and TIDE score was analyzed based on TCGA-SKCM (Spearman method, n = 471). (**C**) Representative co-stained images of NID2, CK, and CD8. According to the spatial distribution of CD8+ T cells. Measures were taken from different samples (Magnification, ×50, scale bars = 200 μm). (**D**) NID2/CD8 immunohistochemistry was performed on consecutive sections. Tumors were sliced as serial 3-μm sections and histologic sections were scored in a blinded manner by 2 pathologists (Magnification, ×400, scale bars = 50 μm). (**E**) The Sankey diagram fully demonstrated the difference in response to immunotherapy between high and low *NID2* expression groups based on GSE91061.

suggest that *NID2* may be associated with poor immunotherapy outcomes, we retrospectively collected 40 SKCM patients and assessed their NID2 and CD8 levels by Immunohistochemistry (IHC), whereas there was no significant correlation between NID2 and CD8 expression level (Figure 9D). GES91061 dataset showed that patients who had high *NID2* levels had more difficulty benefiting from immunotherapy compared to those who had low *NID2* levels (Figure 9E). The results further confirmed that *NID2* is a potential immune exclusion factor.

Discussion

Benefiting from its impressive efficiency and low side effects, Immunotherapy is becoming a pillar of modern cancer treatment.[56] Because melanoma is one of the most immunogenic tumors, it is most likely to respond favorably to immunotherapy.[57,58] However, immunotherapy strategies are not successful in all patients.[59] With the large-scale clinical application of immunotherapy and continuous in-depth research, a large number of mutually synergistic inhibitory mechanisms have been discovered that can help tumor cells evade surveillance and destruction by both intrinsic and adaptive immunity.[60–62] In addition to the "depleted" phenotype of cytotoxic T cells infiltrating the tumor, the physical exclusion of T cells mediated by tumor fibrosis also leads to a downregulation of T cell effector function to weaken tumor immunity.[63,64] The distinguishing feature of tumor fibrosis is the remodeling of the ECM, a complex structure composed of variable members of different protein families.[65,66] The most abundant of these is the collagen family, which contains more than 40 different collagen types.[67] In the present study, we overviewed the transcriptional heterogeneity of 44 collagen molecules at the pan-cancer level and found that the imbalance of collagen molecule expression may be associated with the regulation of genomic variants. We defined two clusters by transcriptome expression profiles of collagen molecules in two separate datasets named Cluster 1 (C1) and Cluster 2 (C2), respectively. We noted that collagen activity was significantly higher in C1 than in C2 and that the distribution of pathological features was significantly different in the two clusters.

It has been well established that changes in the stiffness and density of collagen-rich ECM are associated with tumor cell invasion and metastasis.[68] We found that EMT and angiogenesis signaling were significantly and highly enriched in C1, with the former acting as a key pathway for activating the latter, resulting in both always appearing simultaneously to aid tumor growth and metastasis. It has also been recently shown that high levels of type VI collagen promote EMT, angiogenesis, inflammation, and chemoresistance.[69,70] We then integrated the Differential gene expression (DEG) between the two clusters and constructed the Multiscale Embedded Gene Co-Expression Network Analysis (MEGENA) network, identifying three important gene modules that have strong intersections with each other and are closely associated with ECM-related biological signals. Finally, we included all hub genes in COX regression to further identify reliable prognostic factors and found that overexpression of *ZEB1* and *NID2* predicted poor prognosis in melanoma patients. The importance of *ZEB1* as a star molecule in cancer research in solid tumors needs no elaboration, and notably, *ZEB1* has been found to inhibit CD8+ T cell recruitment in melanoma to promote resistance to anti-PD1 immunotherapy.[71] *NID2*, a new promising tumor marker, is associated with malignant invasion of tumor cells in bladder cancer and gastrointestinal tract tumors.[72–74] Considering that *NID2* has not been characterized in melanoma, we focused our study on *NID2*. Single-cell analysis showed that *NID2* was restrictedly expressed on fibroblasts and endothelial cells and was highly positively correlated with fibroblast abundance. Resident fibroblast populations in TME frequently expand and express proteins specific to their activation state to orchestrate the inflammation that promotes cancer, and it is now generally accepted that fibroblast activation is associated with collagen deposition.[75] Since C1 is notably characterized by high expression of collagen, we speculated that *NID2* may be a potential key regulator. Interestingly, we found that the expression trends of NID2 and most fibroblast activation proteins are consistent, implying that NID2 may be involved in fibroblast activation.

Tumors with high T cell infiltration often referred to as "hot" tumors, are associated with a higher likelihood of responding to immune checkpoint blockade, as opposed to immune cold tumors that show minimal T cell infiltration and typically fail to respond to checkpoint regulation.[76–78] This knowledge has shaped the conceptual framework of "hot" and "cold" tumors and has been the driving force behind the conversion of the so-called cold tumor microenvironment into an immune-active or "hot" microenvironment.[79] However, in clinical practice, a significant proportion of patients with tumors defined as "hot" remain unresponsive or poorly responsive to anti-PD-1/PD-L1 therapy, suggesting that

a more precise biological theory is needed to define mechanisms of therapeutic resistance.[80] Previous studies have demonstrated the ability of TGF-β1 to exert immunosuppressive functions by activating fibroblasts to produce a collagen barrier that protects tumors from immune infiltration.[81,82] We observed a high abundance of stromal cell infiltration, including fibroblasts and endothelial cells, in C1. In addition, it is noteworthy that there was little difference in each immunological index between the two clusters, which strongly suggests that the high degree of mesenchymalization may be the most important reason for the poor prognosis in C1. "ESTIMATE" showed that the stromal score of C1 was much higher than that of C2, while the pathological sections directly confirmed that the tumor tissue of C1 was rich in stroma. It has been demonstrated that the highly grown tumor stroma produces abnormal tumor-stromal signaling under the coercion of the tumor parenchyma thereby limiting the delivery of various drugs as well as immune components, a malignant feature currently considered to be highly associated with the immune exclusion phenotype.[83] Our results suggested that patients with C1 are less likely to benefit from immunotherapy compared to C2.

Considering the close relationship between collagen molecules and immune exclusion and the heterogeneity of collagen molecular phenotypes in melanoma patients, we developed a scoring system, Col_Score, to quantify the expression of collagen molecular factors in tumor patients. Col_Score was highly positively correlated with fibroblast and endothelial cell infiltration, and significantly correlated with EMT progression. In clinical practice, Col_Score can be used to evaluate the expression patterns of collagen molecules and the corresponding infiltration characteristics of stromal cells in melanoma patients, identify the immunophenotype of the tumor, predict the prognosis of the patients, and select the appropriate immunotherapy strategy. Finally, we verified the importance of NID2 in the effect on melanoma stroma growth and immunophenotyping through various experiments. Tumors with high NID2 expression tended to have an immune exclusion phenotype, whereas there was no significant correlation between NID2 and CD8 levels, suggesting an important role of NID2 in collagen-induced immune exclusion.

Our study has some limitations. The current main conclusions rely on second-generation sequencing data, and further analysis of large-scale protein sequencing is needed to verify the clinical feasibility. In addition, we found that NID2 may play an important function in fibrosing interstitial melanoma, but the specific biological mechanisms remain unexplored. Our researchers are conducting an in-depth study on this topic.

Conclusion

In conclusion, our study highlights the relationship between collagen and immune exclusion features of melanoma. These observations may be useful for the treatment of melanoma patients based on immunotherapy. We also identified NID2 as a potential key factor under the collagen phenotype, restricted expression on fibroblasts, and associated with fibroblast activation as an independent prognostic factor in melanoma patients.

Data Sharing Statement

Prof. Hui Shen can be contacted (zjgzy046@njucm.edu.cn) regarding the availability of data and materials.

Ethics Approval and Consent to Participate

The study's protocol was approved by the ethics committee of the Zhangjiagang TCM Hospital Affiliated to Nanjing University of Chinese Medicine, and informed consent was obtained from clinicians and patients (approval number: 2020-78-1). The study was in accordance with the declaration of Helsinki.

Consent for Publication

All authors have given consent for publication.

Acknowledgments

The authors gratefully acknowledge contributions from the GEO and TCGA databases.

Author Contributions

All authors made a significant contribution to the work reported, whether in study conception, design, and execution; data acquisition, analysis, and interpretation; or all these areas. All authors were involved in drafting, revising, or critically reviewing the article; gave final approval for the version to be published; have agreed on the journal to which the article has been submitted; and agree to be accountable for all aspects of the work.

Funding

The present study was supported by the Youth Science and Technology Project of Zhangjiagang (No. ZJGQNKJ202036); Suzhou Science and Education Promotion Health Project (No. KJXW2021065); Natural Science Foundation of China (No. 82205212).

Disclosure

The authors declare no conflicts of interest in this work.

References

1. Strashilov S, Yordanov A. Aetiology and pathogenesis of cutaneous melanoma: current concepts and advances. *Int J Mol Sci*. 2021;22(12):6395. doi:10.3390/ijms22126395
2. Cortez JL, Vasquez J, Wei ML. The impact of demographics, socioeconomics, and health care access on melanoma outcomes. *J Am Acad Dermatol*. 2021;84(6):1677–1683. doi:10.1016/j.jaad.2020.07.125
3. Cuevas LM, Daud AI. Immunotherapy for melanoma. *Semin Cutan Med Surg*. 2018;37(2):127–131. doi:10.12788/j.sder.2018.028
4. Luke JJ, Flaherty KT, Ribas A, et al. Targeted agents and immunotherapies: optimizing outcomes in melanoma. *Nat Rev Clin Oncol*. 2017;14(8):463–482. doi:10.1038/nrclinonc.2017.43
5. Snyder A, Makarov V, Merghoub T, et al. Genetic basis for clinical response to CTLA-4 blockade in melanoma. *N Engl J Med*. 2014;371(23):2189–2199. doi:10.1056/NEJMoa1406498
6. Willsmore ZN, Coumbe BGT, Crescioli S, et al. Combined anti-PD-1 and anti-CTLA-4 checkpoint blockade: treatment of melanoma and immune mechanisms of action. *Eur J Immunol*. 2021;51(3):544–556. doi:10.1002/eji.202048747
7. Wolchok JD, Kluger H, Callahan MK, et al. Nivolumab plus ipilimumab in advanced melanoma. *N Engl J Med*. 2013;369(2):122–133. doi:10.1056/NEJMoa1302369
8. Ott PA, Hodi FS, Robert C. CTLA-4 and PD-1/PD-L1 blockade: new immunotherapeutic modalities with durable clinical benefit in melanoma patients. *Clin Cancer Res*. 2013;19(19):5300–5309. doi:10.1158/1078-0432.CCR-13-0143
9. Tagliaferri L, Lancellotta V, Fionda B, et al. Immunotherapy and radiotherapy in melanoma: a multidisciplinary comprehensive review. *Hum Vaccin Immunother*. 2022;18(3):1903827. doi:10.1080/21645515.2021.1903827
10. Hamid O, Robert C, Daud A, et al. Five-year survival outcomes for patients with advanced melanoma treated with pembrolizumab in KEYNOTE-001. *Ann Oncol*. 2019;30(4):582–588. doi:10.1093/annonc/mdz011
11. Eggermont AMM, Blank CU, Mandalà M, et al. Adjuvant pembrolizumab versus placebo in resected stage III melanoma (EORTC 1325-MG/KEYNOTE-054): distant metastasis-free survival results from a double-blind, randomised, controlled, Phase 3 trial. *Lancet Oncol*. 2021;22(5):643–654. doi:10.1016/S1470-2045(21)00065-6
12. Joyce JA, Fearon DT. T cell exclusion, immune privilege, and the tumor microenvironment. *Science*. 2015;348(6230):74–80. doi:10.1126/science.aaa6204
13. Nakamura K, Smyth MJ. Myeloid immunosuppression and immune checkpoints in the tumor microenvironment. *Cell Mol Immunol*. 2020;17(1):1–12. doi:10.1038/s41423-019-0306-1
14. Marozzi M, Parnigoni A, Negri A, et al. Inflammation, extracellular matrix remodeling, and proteostasis in tumor microenvironment. *Int J Mol Sci*. 2021;22(15):8102. doi:10.3390/ijms22158102
15. Anderson NM, Simon MC. The tumor microenvironment. *Curr Biol*. 2020;30(16):R921–r925. doi:10.1016/j.cub.2020.06.081
16. Huang J, Zhang L, Wan D, et al. Extracellular matrix and its therapeutic potential for cancer treatment. *Signal Transduct Target Ther*. 2021;6(1):153. doi:10.1038/s41392-021-00544-0
17. Chakravarthy A, Khan L, Bensler NP, et al. TGF-β-associated extracellular matrix genes link cancer-associated fibroblasts to immune evasion and immunotherapy failure. *Nat Commun*. 2018;9(1):4692. doi:10.1038/s41467-018-06654-8
18. Peng DH, Rodriguez BL, Diao L, et al. Collagen promotes anti-PD-1/PD-L1 resistance in cancer through LAIR1-dependent CD8(+) T cell exhaustion. *Nat Commun*. 2020;11(1):4520. doi:10.1038/s41467-020-18298-8
19. Theocharis AD, Skandalis SS, Gialeli C, et al. Extracellular matrix structure. *Adv Drug Deliv Rev*. 2016;97:4–27. doi:10.1016/j.addr.2015.11.001
20. Herrera J, Henke CA, Bitterman PB. Extracellular matrix as a driver of progressive fibrosis. *J Clin Invest*. 2018;128(1):45–53. doi:10.1172/JCI93557
21. Kaushik N, Kim S, Suh Y, et al. Proinvasive extracellular matrix remodeling for tumor progression. *Arch Pharm Res*. 2019;42(1):40–47. doi:10.1007/s12272-018-1097-0
22. Abyaneh HS, Regenold M, McKee TD, et al. Towards extracellular matrix normalization for improved treatment of solid tumors. *Theranostics*. 2020;10(4):1960–1980. doi:10.7150/thno.39995
23. Holmes DF, Lu Y, Starborg T, Kadler KE. Collagen fibril assembly and function. *Curr Top Dev Biol*. 2018;130:107–142.
24. Shi R, Zhang Z, Zhu A, et al. Targeting type I collagen for cancer treatment. *Int J Cancer*. 2022;151(5):665–683. doi:10.1002/ijc.33985

25. Zhang J, Liu J, Zhang H, et al. The role of network-forming collagens in cancer progression. *Int J Cancer*. 2022;151(6):833–842. doi:10.1002/ijc.34004
26. Chen Y, Yang S, Tavormina J, et al. Oncogenic collagen I homotrimers from cancer cells bind to α3β1 integrin and impact tumor microbiome and immunity to promote pancreatic cancer. *Cancer Cell*. 2022;40(8):818–834.e9. doi:10.1016/j.ccell.2022.06.011
27. Wang Z, Jensen MA, Zenklusen JC. A Practical Guide to The Cancer Genome Atlas (TCGA). *Methods Mol Biol*. 2016;1418:111–141.
28. Yan K, Lu Y, Yan Z, et al. 9-gene signature correlated with CD8(+) T cell infiltration activated by IFN-γ: a biomarker of immune checkpoint therapy response in melanoma. *Front Immunol*. 2021;12:622563. doi:10.3389/fimmu.2021.622563
29. Zhang C, Li J, Guo Y, et al. Ese-3 inhibits the proliferation, migration, and invasion of HaCaT cells by downregulating PSIP1 and NUCKS1. *Ann Clin Lab Sci*. 2021;51(4):470–486.
30. Gao Y, Li Y, Niu X, et al. Identification and validation of prognostically relevant gene signature in melanoma. *Biomed Res Int*. 2020;2020:5323614. doi:10.1155/2020/5323614
31. Liu Y, Shou Y, Zhu R, et al. Construction and validation of a ferroptosis-related prognostic signature for melanoma based on single-cell RNA sequencing. *Front Cell Dev Biol*. 2022;10:818457. doi:10.3389/fcell.2022.818457
32. Wang X, Chai Z, Li Y, et al. Identification of potential biomarkers for anti-PD-1 therapy in melanoma by weighted correlation network analysis. *Genes*. 2020;11(4):435.
33. Li J, Smalley I, Chen Z, et al. Single-cell characterization of the cellular landscape of acral melanoma identifies novel targets for immunotherapy. *Clin Cancer Res*. 2022;28(10):2131–2146. doi:10.1158/1078-0432.CCR-21-3145
34. Wilkerson MD, Hayes DN. ConsensusClusterPlus: a class discovery tool with confidence assessments and item tracking. *Bioinformatics*. 2010;26(12):1572–1573. doi:10.1093/bioinformatics/btq170
35. Luo D, Liao S, Liu Y, et al. Holliday cross-recognition protein HJURP: association with the tumor microenvironment in hepatocellular carcinoma and with patient prognosis. *Pathol Oncol Res*. 2022;28:1610506. doi:10.3389/pore.2022.1610506
36. Chen X, Chen H, Yao H, et al. Turning up the heat on non-immunoreactive tumors: pyroptosis influences the tumor immune microenvironment in bladder cancer. *Oncogene*. 2021;40(45):6381–6393. doi:10.1038/s41388-021-02024-9
37. Gene Ontology Consortium. Gene Ontology Consortium: going forward. *Nucleic Acids Res*. 2015;43(Database issue):D1049–D1056. doi:10.1093/nar/gku1179
38. Kanehisa M, Goto S. KEGG: Kyoto encyclopedia of genes and genomes. *Nucleic Acids Res*. 2000;28(1):27–30. doi:10.1093/nar/28.1.27
39. Zhou Y, Zhou B, Pache L, et al. Metascape provides a biologist-oriented resource for the analysis of systems-level datasets. *Nat Commun*. 2019;10(1):1523. doi:10.1038/s41467-019-09234-6
40. Hänzelmann S, Castelo R, Guinney J. GSVA: gene set variation analysis for microarray and RNA-seq data. *BMC Bioinform*. 2013;14:7. doi:10.1186/1471-2105-14-7
41. Liberzon A, Birger C, Thorvaldsdóttir H, et al. The molecular signatures database (MSigDB) hallmark gene set collection. *Cell Syst*. 2015;1(6):417–425. doi:10.1016/j.cels.2015.12.004
42. Yang Y, Meyer K, Wind G, et al. Cloud products from the Earth Polychromatic Imaging Camera (EPIC): algorithms and initial evaluation. *Atmos Meas Tech*. 2019;12(3):2019–2031. doi:10.5194/amt-12-2019-2019
43. Wu J, Li L, Zhang H, et al. A risk model developed based on tumor microenvironment predicts overall survival and associates with tumor immunity of patients with lung adenocarcinoma. *Oncogene*. 2021;40(26):4413–4424. doi:10.1038/s41388-021-01853-y
44. Shen Y, Peng X, Shen C. Identification and validation of immune-related lncRNA prognostic signature for breast cancer. *Genomics*. 2020;112(3):2640–2646. doi:10.1016/j.ygeno.2020.02.015
45. Clough E, Barrett T. The gene expression omnibus database. *Methods Mol Biol*. 2016;1418:93–110.
46. Yu X, Zhang Q, Zhang S, et al. Single-cell sequencing and establishment of an 8-gene prognostic model for pancreatic cancer patients. *Front Oncol*. 2022;12:1000447. doi:10.3389/fonc.2022.1000447
47. Kołat D, Kałuzińska Ż, Orzechowska M, et al. Functional genomics of AP-2α and AP-2γ in cancers: in silico study. *BMC Med Genomics*. 2020;13(1):174. doi:10.1186/s12920-020-00823-9
48. Song WM, Zhang B, Wang E. Multiscale embedded gene co-expression network analysis. *PLoS Comput Biol*. 2015;11(11):e1004574. doi:10.1371/journal.pcbi.1004574
49. Magaki S, Hojat SA, Wei B, et al. An introduction to the performance of immunohistochemistry. *Methods Mol Biol*. 2019;1897:289–298.
50. Im K, Mareninov S, Diaz MF, Yong WH. An introduction to performing immunofluorescence staining. *Methods Mol Biol*. 2019;1897:299–311.
51. Yang Y, Xiao M, Song Y, et al. H-score of 11β-hydroxylase and aldosterone synthase in the histopathological diagnosis of adrenocortical tumors. *Endocrine*. 2019;65(3):683–691. doi:10.1007/s12020-019-02022-8
52. World Medical Association. World Medical Association Declaration of Helsinki: ethical principles for medical research involving human subjects. *JAMA*. 2013;310(20):2191–2194. doi:10.1001/jama.2013.281053
53. Jung H, Lee HH, Song KY, et al. Validation of the seventh edition of the American Joint Committee on Cancer TNM staging system for gastric cancer. *Cancer*. 2011;117(11):2371–2378. doi:10.1002/cncr.25778
54. Ritchie ME, Phipson B, Wu D, et al. limma powers differential expression analyses for RNA-sequencing and microarray studies. *Nucleic Acids Res*. 2015;43(7):e47. doi:10.1093/nar/gkv007
55. Wu X, Sui Z, Zhang H, et al. Integrated analysis of lncRNA-mediated ceRNA network in lung adenocarcinoma. *Front Oncol*. 2020;10:554759. doi:10.3389/fonc.2020.554759
56. Riley RS, June CH, Langer R, et al. Delivery technologies for cancer immunotherapy. *Nat Rev Drug Discov*. 2019;18(3):175–196. doi:10.1038/s41573-018-0006-z
57. Herlyn M, Koprowski H. Melanoma antigens: immunological and biological characterization and clinical significance. *Annu Rev Immunol*. 1988;6:283–308. doi:10.1146/annurev.iy.06.040188.001435
58. Marzagalli M, Ebelt ND, Manuel ER. Unraveling the crosstalk between melanoma and immune cells in the tumor microenvironment. *Semin Cancer Biol*. 2019;59:236–250. doi:10.1016/j.semcancer.2019.08.002
59. Versluis JM, Reijers ILM, Rozeman EA, et al. Neoadjuvant ipilimumab plus nivolumab in synchronous clinical stage III melanoma. *Eur J Cancer*. 2021;148:51–57. doi:10.1016/j.ejca.2021.02.012

60. Stachyra-Strawa P, Ciesielka M, Janiszewski M, et al. The role of immunotherapy and molecular-targeted therapy in the treatment of melanoma (Review). *Oncol Rep*. 2021;46(2). doi:10.3892/or.2021.8109
61. Daud A. Current and emerging perspectives on immunotherapy for melanoma. *Semin Oncol*. 2015;42(Suppl 3):S3–S11. doi:10.1053/j.seminoncol.2015.10.003
62. Bari S, Muzaffar J, Eroglu Z. Combination targeted and immune therapy in the treatment of advanced melanoma: a valid treatment option for patients? *Ther Adv Med Oncol*. 2022;14:17588359221090306. doi:10.1177/17588359221090306
63. Madden MZ, Rathmell JC. The complex integration of T-cell metabolism and immunotherapy. *Cancer Discov*. 2021;11(7):1636–1643. doi:10.1158/2159-8290.CD-20-0569
64. Waldman AD, Fritz JM, Lenardo MJ. A guide to cancer immunotherapy: from T cell basic science to clinical practice. *Nat Rev Immunol*. 2020;20(11):651–668. doi:10.1038/s41577-020-0306-5
65. Piersma B, Hayward MK, Weaver VM. Fibrosis and cancer: a strained relationship. *Biochim Biophys Acta Rev Cancer*. 2020;1873(2):188356. doi:10.1016/j.bbcan.2020.188356
66. Mohan V, Das A, Sagi I. Emerging roles of ECM remodeling processes in cancer. *Semin Cancer Biol*. 2020;62:192–200. doi:10.1016/j.semcancer.2019.09.004
67. Rømer AMA, Thorseth ML, Madsen DH. Immune modulatory properties of collagen in cancer. *Front Immunol*. 2021;12:791453. doi:10.3389/fimmu.2021.791453
68. Winkler J, Abisoye-Ogunniyan A, Metcalf KJ, et al. Concepts of extracellular matrix remodelling in tumour progression and metastasis. *Nat Commun*. 2020;11(1):5120. doi:10.1038/s41467-020-18794-x
69. Nissen NI, Karsdal M, Willumsen N. Collagens and cancer associated fibroblasts in the reactive stroma and its relation to cancer biology. *J Exp Clin Cancer Res*. 2019;38(1):115. doi:10.1186/s13046-019-1110-6
70. Li X, Li Z, Gu S, et al. A pan-cancer analysis of collagen VI family on prognosis, tumor microenvironment, and its potential therapeutic effect. *BMC Bioinform*. 2022;23(1):390. doi:10.1186/s12859-022-04951-0
71. Plaschka M, Benboubker V, Grimont M, et al. ZEB1 transcription factor promotes immune escape in melanoma. *J Immunother Cancer*. 2022;10(3):e003484. doi:10.1136/jitc-2021-003484
72. Shan Z, Wang W, Tong Y, et al. Genome-scale analysis identified NID2, SPARC, and MFAP2 as prognosis markers of overall survival in gastric cancer. *Med Sci Monit*. 2021;27:e929558. doi:10.12659/MSM.929558
73. Yu ZH, Wang Y-M, Jiang Y-Z, et al. NID2 can serve as a potential prognosis prediction biomarker and promotes the invasion and migration of gastric cancer. *Pathol Res Pract*. 2019;215(10):152553. doi:10.1016/j.prp.2019.152553
74. Fantony JJ, Longo TA, Gopalakrishna A, et al. Urinary NID2 and TWIST1 methylation to augment conventional urine cytology for the detection of bladder cancer. *Cancer Biomark*. 2017;18(4):381–387. doi:10.3233/CBM-160261
75. Roy B, Yuan L, Lee Y, et al. Fibroblast rejuvenation by mechanical reprogramming and redifferentiation. *Proc Natl Acad Sci U S A*. 2020;117(19):10131–10141. doi:10.1073/pnas.1911497117
76. Liu YT, Sun ZJ. Turning cold tumors into hot tumors by improving T-cell infiltration. *Theranostics*. 2021;11(11):5365–5386. doi:10.7150/thno.58390
77. Bonaventura P, Shekarian T, Alcazer V, et al. Cold tumors: a therapeutic challenge for immunotherapy. *Front Immunol*. 2019;10:168. doi:10.3389/fimmu.2019.00168
78. Lopez de Rodas M, Schalper KA. Tumour antigen-induced T cell exhaustion - The archenemy of immune-hot malignancies. *Nat Rev Clin Oncol*. 2021;18(12):749–750. doi:10.1038/s41571-021-00562-5
79. Fabian KP, Padget MR, Fujii R, et al. Differential combination immunotherapy requirements for inflamed (warm) tumors versus T cell excluded (cool) tumors: engage, expand, enable, and evolve. *J Immunother Cancer*. 2021;9(2):e001691.
80. Taefehshokr S, Parhizkar A, Hayati S, et al. Cancer immunotherapy: challenges and limitations. *Pathol Res Pract*. 2022;229:153723. doi:10.1016/j.prp.2021.153723
81. de Streel G, Bertrand C, Chalon N, et al. Selective inhibition of TGF-β1 produced by GARP-expressing Tregs overcomes resistance to PD-1/PD-L1 blockade in cancer. *Nat Commun*. 2020;11(1):4545. doi:10.1038/s41467-020-17811-3
82. Lodyga M, Hinz B. TGF-β1 - A truly transforming growth factor in fibrosis and immunity. *Semin Cell Dev Biol*. 2020;101:123–139. doi:10.1016/j.semcdb.2019.12.010
83. Costa A, Kieffer Y, Scholer-Dahirel A, et al. Fibroblast heterogeneity and immunosuppressive environment in human breast cancer. *Cancer Cell*. 2018;33(3):463–479.e10. doi:10.1016/j.ccell.2018.01.011